Robotica: (2021) volume 39, pp. 23–41. © Cambridge University Press 2020
doi:10.1017/S0263574720000077

Dynamic Manipulability Analysis of Multi-Arm Space Robot

Yiqun Zhou†‡, Jianjun Luo†‡ and Mingming Wang‡¶*

†*School of Astronautics, Northwestern Polytechnical University, 710072, Xi'an, China*
‡*National Key Laboratory of Aerospace Flight Dynamics, 710072, Xi'an, China*
¶*Qingdao Research Institute of Northwestern Polytechnical University, 266200, Qingdao, China*

(Accepted January 1, 2020. First published online: February 10, 2020)

SUMMARY
The dynamic manipulability of a manipulator refers to the capacity to generate accelerations given the joint torques, which is an important indicator for motion planning and control. In this paper, the dynamic manipulability analysis is extended to the multi-arm space robot, and further to the closed-loop system composed of the space robot and the captured target. According to the dynamic equations, the relation between the joint torques and the end-effector accelerations in the open-loop space robot and that between the joint torques and the target accelerations in the closed-loop system are derived. On this basis, the dynamic manipulability factor and dynamic manipulability ellipsoid are proposed as two tools for the dynamic manipulability measure, where the effects of the bias acceleration are considered. The influences of dynamic parameters, link lengths, joint variables, and velocities on the dynamic manipulability measure are mainly studied.

KEYWORDS: Multi-arm space robot; Closed-loop system; Dynamic manipulability factor; Dynamic manipulability ellipsoid.

1. Introduction

With the development of space technology, more complex space tasks will be carried out in the future. Space robots can replace astronauts in high-risk space tasks such as capturing failure satellites, transporting and assembling large space aircrafts, and cleaning up space debris, which have attracted the attention of the world's major space powers over the past 30 years. A series of studies have been carried out like The Shuttle Remote Manipulator System, Robot Technology Experiment, Engineering Test Satellite VII, Robonaut, etc.[1–5] In view of the above-mentioned facts, an increase in the number and the capacity of robot applied in space explorations will be a foregone conclusion in the coming future.[6,7] Free-floating space robot exhibits some special characteristics due to the dynamic coupling between the space manipulators and the spacecraft (base). Therefore, particular modeling, trajectory planning and control techniques have to be developed to cope with the dynamic coupling issue of free-floating space robot.

The manipulability measure is one of the most important indicators for the manipulator. This concept originally evaluates the mapping from joint velocity to the reference point velocity, that is, the ability to generate the end-effector velocities given the range of joint velocities,[8] which only involves kinematic parameters of the manipulator, and can be called the kinematic manipulability. The kinematic manipulability measure is one of the hot spots in the robot field. Vahrenkamp et al.[9] used manipulability measure to build a quality distribution in workspace. They[10] also proposed an extension to the manipulability measure which incorporates constraining factors. Okada and Tahara[11] used manipulability measure to evaluate the output force of the end point of the manipulator.

* Corresponding author. E-mail: mwang@nwpu.edu.cn

Tanaka et al.[12] proposed a scheme for human force manipulability. The manipulability measure has also been applied in the field of space robot. Wang et al.[13–15] used it as an optimization index and designed different path planning methods to maximize the end-effector manipulability. Chen and Qin[16] established a cost function measurement of key performance characteristics including manipulability. Yan et al.[17,18] introduced it into control problems. Zhang et al.[19,20] proposed a performance index based on the manipulability measure to design and choose an optimization configuration for a dual-arm space robot.

Yoshikawa[21] took the dynamics into consideration and proposed the concept of dynamic manipulability for a single fixed-base manipulator, which is defined as the capacity to generate the end-effector accelerations given the range of joint torques. The DME is proposed to give a measure of the ability of performing end-effector accelerations in a given posture with the joint torques constrained to belong to a unit sphere. Chiacchio[22] proposed a new definition of DME for redundant manipulators which leads to more correct results in evaluating manipulator capabilities in terms of task-space accelerations. Rosenstein and Grupen[23] derived the relationship between joint velocity and end-effector acceleration and explored the dynamic manipulability in motion. Chiacchio et al.[24] also introduced the DME for multi-arm systems. For multiple robotic mechanisms in coordinated manipulation, Lee and Shim[25] derived the bounds of task acceleration of object carried by the system. Yokokohji et al.[26] extended the concept of dynamic manipulability to evaluate the dynamic property of multi-fingered grasping systems consisting of a multi-fingered hand and a grasped object and explored the effects of internal force. Based on the end-effector manipulability, Cotton et al.[27] introduced dynamic manipulability of the center of mass (CoM) for humanoid robots. Gu et al.[28] proposed feasible CoM dynamic manipulability for planar humanoids. Azad et al.[29] analysed CoM dynamic manipulability of floating base robots which have multiple contacts with the environment. In addition, by combining dynamic manipulability and reconfiguration manipulability, Minami et al.[30,31] defined the concept of dynamic reconfiguration manipulability, which estimates dynamic ability to change configuration by using remaining redundancy, while prior task is being controlled. Azad et al.[32] studied the importance of the weighting matrix included in the mapping for dynamic manipulability of robots.

The aforementioned studies about dynamic manipulability mainly focused on ground manipulator. Due to the space microgravity environment, the base of the space robot can be fixed (equal to the ground manipulator), controlled (the free-flying mode), or free (the free-floating mode). The last mode is mainly studied in this paper, which has six more degrees of freedom than the ground manipulator. Unlike the fixed-base robot, a free-floating space robot meets the conservation of momentum, and the movement of manipulators will alter the base. Compared with a single-arm space robot, a multi-arm robot has much more dexterity and flexibility and is capable of carrying out more complex tasks. What is more, when a multi-arm space robot captures the target, a closed-loop system will be formed and its dynamic manipulability measure is more complicated. The study on dynamic manipulability in above conditions is necessary for the design, planning, and control of space robots.

The main contributions of this paper lie in three aspects: (1) We study the dynamic manipulability of the multi-arm space robot and further consider that of a closed-loop system composed of the space robot and the capture target. (2) The spatial vector theory and the graph theory are used to model general space robots, while the dynamic manipulability ellipsoid (DME) and dynamic manipulability factor (DMF) based on singular values of the correlation matrices are presented for dynamic manipulability measure, which take the bias acceleration under the motion state into account. (3) The effects of mass, link lengths, joint variables, and velocities on the dynamic manipulability are mainly studied.

The remainder of this paper is organized as follows. In Section 2, we use the spatial vector theory and the graph theory to model space robots, and the expression of end-effector accelerations about joint torques in the open-loop space robot and the closed-loop system is derived. Two measuring tools, DMF and DME, are presented in Section 3. Finally, Section 4 studies the influences of different factors on dynamic manipulability.

2. Modeling of Space Robots

To derive the kinematic and dynamic equations quickly and express them in a compact form, we use the 6D vectors called spatial vectors,[33,34] which combine the linear and angular aspects of motions

https://doi.org/10.1017/S0263574720000077 Published online by Cambridge University Press

and forces. Then, the graph theory is employed to model general multi-arm space robots, where the connectivity, geometry, and joint model are completely described. The dynamic equations of the open-loop space robot and the closed-loop system are derived as the basis of dynamic manipulability measure and analysis.

2.1. Spatial vector theory

The velocity of body B is composed of a linear velocity $\boldsymbol{v}_O$ and an angular velocity $\boldsymbol{\omega}$ about the axis. The force acting on body B consists of a linear force $\boldsymbol{f}$ and a couple $\boldsymbol{n}_O$ about the axis. The spatial velocity of body B and the spatial force acting on it can be represented as

$$\boldsymbol{V} = \begin{bmatrix} \boldsymbol{\omega} \\ \boldsymbol{v}_O \end{bmatrix}, \qquad \boldsymbol{F} = \begin{bmatrix} \boldsymbol{n}_O \\ \boldsymbol{f} \end{bmatrix} \tag{1}$$

A spatial velocity is the combination of angular velocity and linear velocity, while a spatial force is the combination of couple and linear force.

The matrix $\boldsymbol{E}_A^B \in \mathbb{R}^{3\times3}$ represents a rotation transform for 3D vectors from frame A to B. Let $\boldsymbol{X}_A^B \in \mathbb{R}^{6\times6}$ and $\boldsymbol{Y}_A^B \in \mathbb{R}^{6\times6}$ be the same transforms for spatial motion and spatial force vectors, respectively, which are related by $\boldsymbol{Y}_A^B = (\boldsymbol{X}_A^B)^{-\mathrm{T}}$. Their forms are

$$\boldsymbol{X}_A^B = \begin{bmatrix} \boldsymbol{E}_A^B & \boldsymbol{0} \\ \boldsymbol{0} & \boldsymbol{E}_A^B \end{bmatrix} \begin{bmatrix} \boldsymbol{1} & \boldsymbol{0} \\ -\boldsymbol{r}\times & \boldsymbol{1} \end{bmatrix} = \begin{bmatrix} \boldsymbol{E}_A^B & \boldsymbol{0} \\ -\boldsymbol{E}_A^B\boldsymbol{r}\times & \boldsymbol{E}_A^B \end{bmatrix} \tag{2}$$

and

$$\boldsymbol{Y}_A^B = \begin{bmatrix} \boldsymbol{E}_A^B & \boldsymbol{0} \\ \boldsymbol{0} & \boldsymbol{E}_A^B \end{bmatrix} \begin{bmatrix} \boldsymbol{1} & -\boldsymbol{r}\times \\ \boldsymbol{0} & \boldsymbol{1} \end{bmatrix} = \begin{bmatrix} \boldsymbol{E}_A^B & -\boldsymbol{E}_A^B\boldsymbol{r}\times \\ \boldsymbol{0} & \boldsymbol{E}_A^B \end{bmatrix} \tag{3}$$

where $\mathbf{0}$ and $\mathbf{1}$ are zero and identity matrix, $\boldsymbol{r}\times$ is the cross product operator for $\boldsymbol{r} = \overrightarrow{AB}$ (expressed in frame A)

$$\boldsymbol{r}\times = \begin{bmatrix} 0 & -r_z & r_y \\ r_z & 0 & -r_x \\ -r_y & r_x & 0 \end{bmatrix} \tag{4}$$

The spatial acceleration is the time derivative of its spatial velocity

$$\dot{\boldsymbol{V}} = \begin{bmatrix} \dot{\boldsymbol{\omega}} \\ \dot{\boldsymbol{v}}_O \end{bmatrix} = \begin{bmatrix} \dot{\boldsymbol{\omega}} \\ \ddot{\boldsymbol{p}} - \boldsymbol{\omega} \times \boldsymbol{v}_O \end{bmatrix} \tag{5}$$

where $\boldsymbol{p}$ is the position of O.

If a body has the mass of m and the inertia of $\bar{\boldsymbol{I}}_C \in \mathbb{R}^{3\times3}$ about its centroid, its spatial inertia $\boldsymbol{I}_O \in \mathbb{R}^{6\times6}$ about any point O is

$$\boldsymbol{I}_O = \begin{bmatrix} \bar{\boldsymbol{I}}_C - m\boldsymbol{c} \times \boldsymbol{c}\times & m\boldsymbol{c}\times \\ -m\boldsymbol{c}\times & m\boldsymbol{1} \end{bmatrix} \tag{6}$$

where $\boldsymbol{c} = \overrightarrow{OC}$. The derivative of spatial inertia $\boldsymbol{I}$ is

$$\frac{d}{dt}\boldsymbol{I} = \boldsymbol{V} \times^* \boldsymbol{I} - \boldsymbol{I}\boldsymbol{V}\times \tag{7}$$

where $\boldsymbol{V}\times$ and $\boldsymbol{V}\times^*$ represent the cross product operator for spatial velocity and force vectors, whose forms are

$$\boldsymbol{V}\times = \begin{bmatrix} \boldsymbol{\omega}\times & \boldsymbol{0} \\ \boldsymbol{v}_O\times & \boldsymbol{\omega}\times \end{bmatrix} \qquad \boldsymbol{V}\times^* = \begin{bmatrix} \boldsymbol{\omega}\times & \boldsymbol{v}_O\times \\ \boldsymbol{0} & \boldsymbol{\omega}\times \end{bmatrix} = -(\boldsymbol{V}\times)^{\mathrm{T}} \tag{8}$$

https://doi.org/10.1017/S0263574720000077 Published online by Cambridge University Press

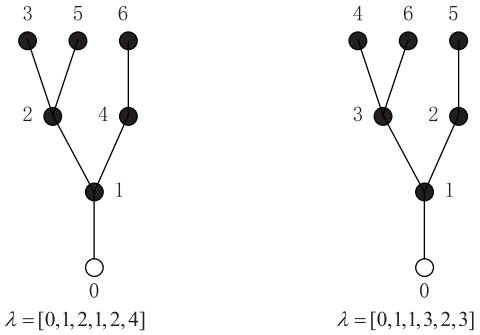

Fig. 1. Two numberings of a simple tree and their corresponding parent arrays.

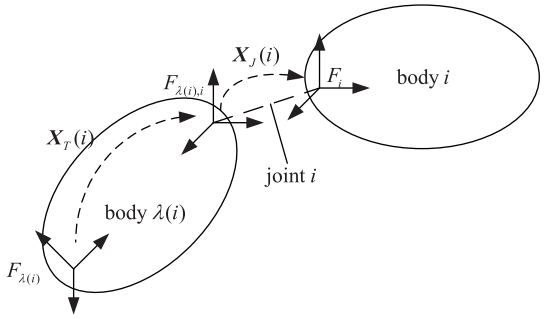

Fig. 2. Coordinate frames and transforms associated with joint i.

The transform for $\boldsymbol{I}$ from frame A to B is

$$\boldsymbol{I}^B = \boldsymbol{Y}_A^B \boldsymbol{I}^A \boldsymbol{X}_B^A \tag{9}$$

Finally, we can get the equation of motion by differentiating the momentum

$$\boldsymbol{F} = \frac{d}{dt}\boldsymbol{I}\boldsymbol{V} = \boldsymbol{I}\dot{\boldsymbol{V}} + (\boldsymbol{V} \times^* \boldsymbol{I} - \boldsymbol{I}\boldsymbol{V}\times)\boldsymbol{V} = \boldsymbol{I}\dot{\boldsymbol{V}} + \boldsymbol{V} \times^* \boldsymbol{I}\boldsymbol{V} \tag{10}$$

2.2. Kinematic modeling

2.2.1. Connectivity. The connectivity of a robot mechanism can be represented by a kinematic tree, where the nodes and arcs represent bodies and joints, respectively. An open-loop space robot is composed of N joints and $N+1$ bodies (including N links and the base) and has M manipulators. The base is assigned the number 0, and the remaining bodies and joints are numbered from 1 to N, respectively, while confirm that each body has a higher number than its parent, and joint i connects body i and its parent. As shown in Fig. 1, the numbering for a certain robotic system is not unique.

The connectivity can be described by arrays. Let $\lambda(i)$ represents the parent of body i, $\mu(i)$ is the set of children of body i, $\kappa(i)$ is the set of joints on the path between body i and the base, and $\nu(i)$ is the set of bodies in the subtree starting at body i. For the left tree of Fig. 1, we have $\lambda(1) = 0$, $\mu(1) = \{2, 4\}$, $\kappa(1) = \{1\}$, $\nu(1) = \{1, 2, 3, 4, 5, 6\}$ and so on. In addition, we use $\varepsilon(j)$ to present the end number of the j^{th} manipulator, and $\varepsilon = \{3, 5, 6\}$ for the left tree of Fig. 1.

2.2.2. Geometry. The geometric model of a robot specifies the relative locations of the joints in each body. As shown in Fig. 2, two coordinate frames are connected by joint i, where the body frame F_i is fixed in body i, and the transition frame $F_{\lambda(i),i}$ is fixed in body $\lambda(i)$. The base frame F_0 is located in its centroid. An end frame $F_{e(j)}$ is defined at the end-effector of the j^{th} manipulator. In general, there are $2N + 1 + M$ coordinate frames on a space robotic system, consisting of $N + 1$ body frames, N transition frames, and M end frames.

https://doi.org/10.1017/S0263574720000077 Published online by Cambridge University Press

The transform $\boldsymbol{X}^{i}_{\lambda(i)}$ from frame $F_{\lambda(i)}$ to F_i can be divided into the transform $\boldsymbol{X}_T(i)$ from frame $F_{\lambda(i)}$ to $F_{\lambda(i),i}$, and the transform $\boldsymbol{X}_J(i)$ from frame $F_{\lambda(i),i}$ to F_i. Their relationship is $\boldsymbol{X}^{i}_{\lambda(i)} = \boldsymbol{X}_J(i)\boldsymbol{X}_T(i)$. $\boldsymbol{X}_J(i)$ is a function of the joint variable q_i. $\boldsymbol{X}_T(i)$ depends on the relative posture and position between $F_{\lambda(i)}$ and $F_{\lambda(i),i}$, which is a constant. In addition, the transform $\boldsymbol{X}_E(j)$ from end body frame $F_{\varepsilon(j)}$ to the end frame $F_{e(j)}$ (noticing that they are two different frames) is also a constant.

2.2.3. Joint model. A joint is a kinematic constraint between two bodies, which can be indicated by the joint subspace $\boldsymbol{S}_i$. The frames $F_{\lambda(i),i}$ and F_i have a common z axis, and coincide when $q_i = 0$. For a revolute (R) joint i, the joint subspace is $\boldsymbol{S}_i = \begin{bmatrix}0\ 0\ 1\ 0\ 0\ 0\end{bmatrix}^{\mathrm{T}}$, meaning that frame F_i can only rotate relative to frame $F_{\lambda(i),i}$ about the common z axis, and q_i is the rotation angle. For a prismatic (P) joint i, the joint subspace is $\boldsymbol{S}_i = \begin{bmatrix}0\ 0\ 0\ 0\ 0\ 1\end{bmatrix}^{\mathrm{T}}$, meaning that frame F_i can only translate relative to frame $F_{\lambda(i),i}$ along the common z axis, and q_i is the translation distance.

The velocity of each body (expressed in its body frame) is composed of the velocity transmitted from the parent body and the joint velocity

$$\boldsymbol{V}_i = \boldsymbol{X}^{i}_{\lambda(i)}\boldsymbol{V}_{\lambda(i)} + \boldsymbol{S}_i\dot{q}_i \tag{11}$$

On the basis of Eq. (11), we can get the velocity of each body starting from the base. The end velocities are derived by

$$\begin{aligned}
\boldsymbol{V}_{e(j)} &= \boldsymbol{X}_E(j)\boldsymbol{V}_{\varepsilon(j)} \\
&= \boldsymbol{X}_E(j)(\boldsymbol{S}_{\varepsilon(j)}\dot{q}_{\varepsilon(j)} + \boldsymbol{X}^{\varepsilon(j)}_{\lambda(\varepsilon(j))}\boldsymbol{S}_{\lambda(\varepsilon(j))}\dot{q}_{\lambda(\varepsilon(j))} + \cdots + \boldsymbol{X}^{\varepsilon(j)}_{0}\boldsymbol{V}_0) \\
&= \boldsymbol{X}^{e(j)}_{0}\boldsymbol{V}_0 + \sum_{i\in\kappa(\varepsilon(j))} \boldsymbol{X}^{e(j)}_{i}\boldsymbol{S}_i\dot{q}_i \\
&= \begin{bmatrix}\boldsymbol{J}_{eb(j)}\ \boldsymbol{J}_{em(j)}\end{bmatrix}\begin{bmatrix}\boldsymbol{V}_0 \\ \dot{\boldsymbol{q}}\end{bmatrix} \\
&= \boldsymbol{J}_{e(j)}\dot{\boldsymbol{x}}
\end{aligned} \tag{12}$$

where $\dot{\boldsymbol{x}} \in \mathbb{R}^{6+N}$ is the general velocity of the space robot, and $\boldsymbol{J}_{e(j)} \in \mathbb{R}^{6\times(6+N)}$ is the end Jacobian for the j^{th} manipulator, which can be lined up as

$$\boldsymbol{V}_e = \begin{bmatrix}\boldsymbol{V}_{e(1)} \\ \vdots \\ \boldsymbol{V}_{e(M)}\end{bmatrix} = \begin{bmatrix}\boldsymbol{J}_{eb(1)} & \boldsymbol{J}_{em(1)} \\ \vdots & \vdots \\ \boldsymbol{J}_{eb(M)} & \boldsymbol{J}_{em(M)}\end{bmatrix}\begin{bmatrix}\boldsymbol{V}_0 \\ \dot{\boldsymbol{q}}\end{bmatrix} = \begin{bmatrix}\boldsymbol{J}_{eb} & \boldsymbol{J}_{em}\end{bmatrix}\begin{bmatrix}\boldsymbol{V}_0 \\ \dot{\boldsymbol{q}}\end{bmatrix} = \boldsymbol{J}_e\dot{\boldsymbol{x}} \tag{13}$$

where $\boldsymbol{J}_e \in \mathbb{R}^{6M\times(6+N)}$ is the end Jacobian of the whole robotic system.

In general, the symbols used in this paper are listed in Table I. Without special explanation, the vectors and matrices related to body i are expressed in frame F_i.

2.3. Dynamic modeling

2.3.1. Dynamic equation of the open-loop space robot. The dynamic equation of a space robotic system using Lagrangian mechanism can be expressed as follows:

$$\boldsymbol{H}\ddot{\boldsymbol{x}} + \boldsymbol{C} = \boldsymbol{T} - \boldsymbol{J}_e^{\mathrm{T}}\boldsymbol{F}_e \tag{14}$$

which can be decomposed into the form

$$\begin{bmatrix}\boldsymbol{H}_b & \boldsymbol{H}_{bm} \\ \boldsymbol{H}_{bm}^{\mathrm{T}} & \boldsymbol{H}_m\end{bmatrix}\begin{bmatrix}\dot{\boldsymbol{V}}_0 \\ \ddot{\boldsymbol{q}}\end{bmatrix} + \begin{bmatrix}\boldsymbol{C}_b \\ \boldsymbol{C}_m\end{bmatrix} = \begin{bmatrix}\boldsymbol{F}_b \\ \boldsymbol{\tau}\end{bmatrix} - \begin{bmatrix}\boldsymbol{J}_{eb}^{\mathrm{T}} \\ \boldsymbol{J}_{em}^{\mathrm{T}}\end{bmatrix}\boldsymbol{F}_e \tag{15}$$

https://doi.org/10.1017/S0263574720000077 Published online by Cambridge University Press

Table I. Symbols of the space robotic system.

Symbols	Physical meanings
$\lambda(i)$	Parent of body i
$\mu(i)$	Set of children of body i
$\kappa(i)$	Set of joints that support body i
$\nu(i)$	Set of bodies in subtree starting at body i
$\varepsilon(j)$	End-effector of the $j-th$ manipulator
$\alpha_i, \beta_i, \gamma_i$	Euler rotation angles from $F_{\lambda(i)}$ to $F_{\lambda(i),i}$
$\boldsymbol{r}_i$	Vector from $F_{\lambda(i)}$ to $F_{\lambda(i),i}$ expressed in $F_{\lambda(i)}$
$\boldsymbol{c}_i$	Vector from $F_{\lambda(i)}$ to body i's centroid expressed in $F_{\lambda(i)}$
$m_i, \bar{\boldsymbol{I}}_i$	Mass, rotational inertia about the centroid of body i
$\boldsymbol{I}_i, \boldsymbol{M}_i$	Spatial inertia tensor and momentum of body i
$\boldsymbol{X}_A^B, \boldsymbol{Y}_A^B$	6×6 Transform for spatial motion and spatial force vectors
$\boldsymbol{\omega}_i, \boldsymbol{v}_i, \boldsymbol{V}_i$	Angular, linear, and spatial velocity of body i
$\dot{\boldsymbol{\omega}}_i, \dot{\boldsymbol{v}}_i, \dot{\boldsymbol{V}}_i$	Angular, linear, and spatial acceleration of body i
$q_i, \dot{q}_i, \ddot{q}_i$	Variable, velocity, and acceleration of joint i
$\boldsymbol{n}_i, \boldsymbol{f}_i, \boldsymbol{F}_i$	Couple, linear, and spatial force applied to body i
$\boldsymbol{S}_i, \boldsymbol{\tau}_i$	Subspace and torque of joint i
$\boldsymbol{J}_e, \boldsymbol{J}_{eb}, \boldsymbol{J}_{em}$	Jacobian of end-effectors and its components
$\boldsymbol{H}_b, \boldsymbol{H}_m, \boldsymbol{H}_{bm}$	Inertia matrix of base and manipulators, the coupling term

$\boldsymbol{H} \in \mathbb{R}^{(6+N)\times(6+N)}$ is the generalized inertia matrix consisting of the base term $\boldsymbol{H}_b$, the manipulator term $\boldsymbol{H}_m$, and the coupling term between base and manipulators $\boldsymbol{H}_{bm}$. Their detailed forms are

$$\begin{aligned} \boldsymbol{H}_b &= \boldsymbol{I}_0 + \sum_{k=1}^{N} \boldsymbol{Y}_k^0 \boldsymbol{I}_k \boldsymbol{X}_0^k \\ (\boldsymbol{H}_{bm})_j &= \left(\sum_{k\in\nu(j)} \boldsymbol{Y}_k^0 \boldsymbol{I}_k \right) \boldsymbol{X}_j^k \boldsymbol{S}_j \\ (\boldsymbol{H}_m)_{ij} &= \boldsymbol{S}_i^{\mathrm{T}} \left(\sum_{k\in\nu(i)\cap\nu(j)} \boldsymbol{Y}_k^i \boldsymbol{I}_k \boldsymbol{X}_j^k \right) \boldsymbol{S}_j \end{aligned} \tag{16}$$

where $(\boldsymbol{H}_{bm})_j$ is the j^{th} column of $\boldsymbol{H}_{bm}$, and $(\boldsymbol{H}_m)_{ij}$ is the i^{th} row and j^{th} column of $\boldsymbol{H}_m$.

$\boldsymbol{C} \in \mathbb{R}^{6+N}$ is the generalized bias force consisting of the base term $\boldsymbol{C}_b$ and the manipulator term $\boldsymbol{C}_m$. Their detailed forms are

$$\begin{aligned} \boldsymbol{C}_b &= \sum_{i=1}^{N} \boldsymbol{Y}_i^0 \left(\boldsymbol{I}_i \sum_{j\in\kappa(i)} (\boldsymbol{X}_j^i \boldsymbol{V}_j \times \boldsymbol{S}_j \dot{q}_j + \boldsymbol{V}_j \times^* \boldsymbol{I}_j \boldsymbol{V}_j) \right) \\ (\boldsymbol{C}_m)_i &= \boldsymbol{S}_i^{\mathrm{T}} \sum_{j\in\nu(i)} \boldsymbol{Y}_j^i \boldsymbol{I}_j \sum_{k\in\kappa(j)} (\boldsymbol{X}_k^j \boldsymbol{V}_k \times \boldsymbol{S}_k \dot{q}_k + \boldsymbol{V}_k \times^* \boldsymbol{I}_k \boldsymbol{V}_k) \end{aligned} \tag{17}$$

where $(\boldsymbol{C}_m)_i$ is the i^{th} row of $\boldsymbol{C}_m$.

$\boldsymbol{T} \in \mathbb{R}^{6+N}$ is the generalized force exerted on the robotic system consisting of the spatial force acted on the base $\boldsymbol{F}_b$ ($\boldsymbol{F}_b = \boldsymbol{0}$ for a free-floating space robot) and joint torque vector $\boldsymbol{\tau}$. $\boldsymbol{F}_e \in \mathbb{R}^{6M}$ is the space forces exerted on the external environment by end-effectors.

2.3.2. Dynamic equation of the closed-loop system. A closed-loop system is formed after a multi-arm space robot captures the target. The motion equation of the target is

$$\boldsymbol{I}_t \dot{\boldsymbol{V}}_t + \boldsymbol{V}_t \times^* \boldsymbol{I}_t \boldsymbol{V}_t = \boldsymbol{J}_t^{\mathrm{T}} \boldsymbol{F}_e \tag{18}$$

https://doi.org/10.1017/S0263574720000077 Published online by Cambridge University Press

where $\boldsymbol{I}_t$ is the spatial inertia of the target, $\boldsymbol{V}_t$ is the spatial velocity of the target's centroid, and $\boldsymbol{J}_t \in \mathbb{R}^{6M\times 6}$ is the target's Jacobian consisting of transforms from the its centroid to capture points, which is a constant.

The end-effectors of manipulators coincide with the capture points on the target, meaning that their velocities are always the same

$$\boldsymbol{J}_e\dot{\boldsymbol{x}} = \boldsymbol{J}_t\boldsymbol{V}_t \tag{19}$$

The time derivative of Eq. (19) gives the relation of accelerations

$$\boldsymbol{J}_e\ddot{\boldsymbol{x}} + \dot{\boldsymbol{J}}_e\dot{\boldsymbol{x}} = \boldsymbol{J}_t\dot{\boldsymbol{V}}_t \tag{20}$$

Pre-multiplying Eq. (14) by $\boldsymbol{J}_e\boldsymbol{H}^{-1}$, we can obtain

$$\boldsymbol{J}_e\ddot{\boldsymbol{x}} + \boldsymbol{J}_e\boldsymbol{H}^{-1}\boldsymbol{C} = \boldsymbol{J}_e\boldsymbol{H}^{-1}(\boldsymbol{T} - \boldsymbol{J}_e^{\mathrm{T}}\boldsymbol{F}_e) \tag{21}$$

Substituting Eq. (21) into Eq. (20), we get

$$\boldsymbol{J}_t\dot{\boldsymbol{V}}_t + \boldsymbol{J}_e\boldsymbol{H}^{-1}\boldsymbol{J}_e^{\mathrm{T}}\boldsymbol{F}_e = \boldsymbol{J}_e\boldsymbol{H}^{-1}(\boldsymbol{T} - \boldsymbol{C}) + \dot{\boldsymbol{J}}_e\dot{\boldsymbol{x}} \tag{22}$$

Finally, combining Eqs. (18) and (22)

$$\begin{bmatrix} \boldsymbol{I}_t & -\boldsymbol{J}_t^{\mathrm{T}} \\ -\boldsymbol{J}_t & \boldsymbol{P} \end{bmatrix}\begin{bmatrix} \dot{\boldsymbol{V}}_t \\ \boldsymbol{F}_e \end{bmatrix} = \begin{bmatrix} -\boldsymbol{V}_t \times^* \boldsymbol{I}_t\boldsymbol{V}_t \\ \boldsymbol{Q} \end{bmatrix} \tag{23}$$

where $\boldsymbol{P} = -\boldsymbol{J}_e\boldsymbol{H}^{-1}\boldsymbol{J}_e^{\mathrm{T}}$, $\boldsymbol{Q} = -\boldsymbol{J}_e\boldsymbol{H}^{-1}(\boldsymbol{T} - \boldsymbol{C}) - \dot{\boldsymbol{J}}_e\dot{\boldsymbol{x}}$.

Equation (23) is the closed-loop system dynamic equation, which solves $\dot{\boldsymbol{V}}_t$ and $\boldsymbol{F}_e$, and $\ddot{\boldsymbol{x}}$ can be obtained by Eq. (14).

3. Dynamic Manipulability Modeling and Measuring

Yoshikawa[8,21] proposed the manipulability measure $w = \sqrt{\det(\boldsymbol{J}\boldsymbol{J})^{\mathrm{T}}}$ and dynamic manipulability measure $w = \sqrt{\det(\boldsymbol{J}(\boldsymbol{H}^{\mathrm{T}}\boldsymbol{H})^{-1}\boldsymbol{J})^{\mathrm{T}}}$ for the fixed-base manipulator. In this section, the dynamic manipulability of the effectors in the open-loop space robot and the target in the closed-loop system are modeled. To measure the dynamic manipulability, the DME and DMF are proposed and modified based on dynamic manipulability equations.

3.1. Dynamic manipulability modeling

3.1.1. Dynamic manipulability modeling of the open-loop space robot. The dynamic manipulability for end-effectors of the open-loop space robot is considered first. For a free-floating space robot, from Eq. (15), we get

$$\begin{bmatrix} \dot{\boldsymbol{V}}_0 \\ \ddot{\boldsymbol{q}} \end{bmatrix} = \begin{bmatrix} \boldsymbol{H}_b & \boldsymbol{H}_{bm} \\ \boldsymbol{H}_{bm}^{\mathrm{T}} & \boldsymbol{H}_m \end{bmatrix}^{-1}\left(\begin{bmatrix} \boldsymbol{0} \\ \boldsymbol{\tau} \end{bmatrix} - \begin{bmatrix} \boldsymbol{C}_b \\ \boldsymbol{C}_m \end{bmatrix}\right) \tag{24}$$

where $\boldsymbol{F}_b = \boldsymbol{0}$ and $\boldsymbol{F}_e = \boldsymbol{0}$. The time derivative of Eq. (13) is

$$\dot{\boldsymbol{V}}_e = \begin{bmatrix} \boldsymbol{J}_{eb} & \boldsymbol{J}_{em} \end{bmatrix}\begin{bmatrix} \dot{\boldsymbol{V}}_0 \\ \ddot{\boldsymbol{q}} \end{bmatrix} + \begin{bmatrix} \dot{\boldsymbol{J}}_{eb} & \dot{\boldsymbol{J}}_{em} \end{bmatrix}\begin{bmatrix} \boldsymbol{V}_0 \\ \dot{\boldsymbol{q}} \end{bmatrix} \tag{25}$$

Substituting Eq. (25) into Eq. (24)

$$\dot{\boldsymbol{V}}_e = \begin{bmatrix} \boldsymbol{J}_{eb} & \boldsymbol{J}_{em} \end{bmatrix}\begin{bmatrix} \boldsymbol{H}_b & \boldsymbol{H}_{bm} \\ \boldsymbol{H}_{bm}^{\mathrm{T}} & \boldsymbol{H}_m \end{bmatrix}^{-1}\left(\begin{bmatrix} \boldsymbol{0} \\ \boldsymbol{\tau} \end{bmatrix} - \begin{bmatrix} \boldsymbol{C}_b \\ \boldsymbol{C}_m \end{bmatrix}\right) + \begin{bmatrix} \dot{\boldsymbol{J}}_{eb} & \dot{\boldsymbol{J}}_{em} \end{bmatrix}\begin{bmatrix} \boldsymbol{V}_0 \\ \dot{\boldsymbol{q}} \end{bmatrix} \tag{26}$$

Here we define the matrix

$$\boldsymbol{B} = \begin{bmatrix} \boldsymbol{B}_b & \boldsymbol{B}_{bm} \\ \boldsymbol{B}_{bm}^{\mathrm{T}} & \boldsymbol{B}_m \end{bmatrix} = \begin{bmatrix} \boldsymbol{H}_b & \boldsymbol{H}_{bm} \\ \boldsymbol{H}_{bm}^{\mathrm{T}} & \boldsymbol{H}_m \end{bmatrix}^{-1} \tag{27}$$

https://doi.org/10.1017/S0263574720000077 Published online by Cambridge University Press

where

$$\begin{aligned}\boldsymbol{B}_b &= \left(\boldsymbol{H}_b - \boldsymbol{H}_{bm}\boldsymbol{H}_m^{-1}\boldsymbol{H}_{bm}^{\mathrm{T}}\right)^{-1}\\ \boldsymbol{B}_{bm} &= -\left(\boldsymbol{H}_b - \boldsymbol{H}_{bm}\boldsymbol{H}_m^{-1}\boldsymbol{H}_{bm}^{\mathrm{T}}\right)^{-1}\boldsymbol{H}_{bm}\boldsymbol{H}_m^{-1} = -\boldsymbol{B}_b\boldsymbol{H}_{bm}\boldsymbol{H}_m^{-1}\\ \boldsymbol{B}_m &= \boldsymbol{H}_m^{-1} + \boldsymbol{H}_m^{-1}\boldsymbol{H}_{bm}^{\mathrm{T}}\boldsymbol{B}_b\boldsymbol{H}_{bm}\boldsymbol{H}_m^{-1} = \boldsymbol{H}_m^{-1} - \boldsymbol{H}_m^{-1}\boldsymbol{H}_{bm}^{\mathrm{T}}\boldsymbol{B}_{bm}\end{aligned} \tag{28}$$

So we can obtain

$$\begin{aligned}\dot{\boldsymbol{V}}_e &= \left(\boldsymbol{J}_{eb}\boldsymbol{B}_{bm} + \boldsymbol{J}_{em}\boldsymbol{B}_m\right)\boldsymbol{\tau} - \boldsymbol{J}_{eb}\left(\boldsymbol{B}_b\boldsymbol{C}_b + \boldsymbol{B}_{bm}\boldsymbol{C}_m\right)\\ &\quad - \boldsymbol{J}_{em}\left(\boldsymbol{B}_{bm}^{\mathrm{T}}\boldsymbol{C}_b + \boldsymbol{B}_m\boldsymbol{C}_m\right) + \dot{\boldsymbol{J}}_{eb}\boldsymbol{V}_0 + \dot{\boldsymbol{J}}_{em}\dot{\boldsymbol{q}}\\ &= \boldsymbol{Ma}_e\boldsymbol{\tau} + \boldsymbol{b}_e\end{aligned} \tag{29}$$

where $\boldsymbol{Ma}_e = \boldsymbol{J}_{eb}\boldsymbol{B}_{bm} + \boldsymbol{J}_{em}\boldsymbol{B}_m \in \mathbb{R}^{6M\times N}$ is the dynamic manipulability matrix of the end-effectors. $\boldsymbol{b}_e = \dot{\boldsymbol{J}}_{em}\dot{\boldsymbol{q}} - \boldsymbol{J}_{eb}(\boldsymbol{B}_b\boldsymbol{C}_b + \boldsymbol{B}_{bm}\boldsymbol{C}_m) - \boldsymbol{J}_{em}(\boldsymbol{B}_{bm}^{\mathrm{T}}\boldsymbol{C}_b + \boldsymbol{B}_m\boldsymbol{C}_m) + \dot{\boldsymbol{J}}_{eb}\boldsymbol{V}_0 \in \mathbb{R}^{6M}$ is the bias acceleration caused by Coriolis and centrifugal forces, which will be zero if the system is at rest.

Equation (29) can be divided into the form of each manipulator

$$\begin{bmatrix}\dot{\boldsymbol{V}}_{e(1)}\\ \vdots\\ \dot{\boldsymbol{V}}_{e(M)}\end{bmatrix} = \begin{bmatrix}\boldsymbol{Ma}_{e(1)}\\ \vdots\\ \boldsymbol{Ma}_{e(M)}\end{bmatrix}\boldsymbol{\tau} + \begin{bmatrix}\boldsymbol{b}_{e(1)}\\ \vdots\\ \boldsymbol{b}_{e(M)}\end{bmatrix} \tag{30}$$

which also consists of the angular and linear terms

$$\dot{\boldsymbol{V}}_{e(i)} = \begin{bmatrix}\dot{\boldsymbol{\omega}}_{e(i)}\\ \dot{\boldsymbol{\upsilon}}_{e(i)}\end{bmatrix} = \begin{bmatrix}\boldsymbol{Ma}_{e(i)}^{\omega}\\ \boldsymbol{Ma}_{e(i)}^{\upsilon}\end{bmatrix}\boldsymbol{\tau} + \begin{bmatrix}\boldsymbol{b}_{e(i)}^{\omega}\\ \boldsymbol{b}_{e(i)}^{\upsilon}\end{bmatrix} \tag{31}$$

3.1.2. Dynamic manipulability modeling of the closed-loop system. For the closed-loop system, starting from Eq. (23)

$$\begin{bmatrix}\dot{\boldsymbol{V}}_t\\ \boldsymbol{F}_e\end{bmatrix} = \begin{bmatrix}\boldsymbol{I}_t & -\boldsymbol{J}_t^{\mathrm{T}}\\ -\boldsymbol{J}_t & \boldsymbol{P}\end{bmatrix}^{-1}\begin{bmatrix}-\boldsymbol{V}_t \times^* \boldsymbol{I}_t\boldsymbol{V}_t\\ \boldsymbol{Q}\end{bmatrix} \tag{32}$$

Defining the matrix

$$\boldsymbol{G} = \begin{bmatrix}\boldsymbol{G}_t & \boldsymbol{G}_{te}\\ \boldsymbol{G}_{te}^{\mathrm{T}} & \boldsymbol{G}_e\end{bmatrix} = \begin{bmatrix}\boldsymbol{I}_t & -\boldsymbol{J}_t^{\mathrm{T}}\\ -\boldsymbol{J}_t & \boldsymbol{P}\end{bmatrix}^{-1} \tag{33}$$

where

$$\begin{aligned}\boldsymbol{G}_t &= \left(\boldsymbol{I}_t - \boldsymbol{J}_t^{\mathrm{T}}\boldsymbol{P}^{-1}\boldsymbol{J}_t\right)^{-1}\\ \boldsymbol{G}_{te} &= \left(\boldsymbol{I}_t - \boldsymbol{J}_t^{\mathrm{T}}\boldsymbol{P}^{-1}\boldsymbol{J}_t\right)^{-1}\boldsymbol{J}_t^{\mathrm{T}}\boldsymbol{P}^{-1} = \boldsymbol{G}_t\boldsymbol{J}_t^{\mathrm{T}}\boldsymbol{P}^{-1}\\ \boldsymbol{G}_e &= \boldsymbol{P}^{-1} + \boldsymbol{P}^{-1}\boldsymbol{J}_t\boldsymbol{G}_t\boldsymbol{J}_t^{\mathrm{T}}\boldsymbol{P}^{-1} = \boldsymbol{P}^{-1} + \boldsymbol{P}^{-1}\boldsymbol{J}_t\boldsymbol{G}_{te}\end{aligned} \tag{34}$$

So we can obtain

$$\begin{aligned}\dot{\boldsymbol{V}}_t &= -\boldsymbol{G}_{te}\left(\boldsymbol{J}_{eb}\boldsymbol{B}_{bm} + \boldsymbol{J}_{em}\boldsymbol{B}_m\right)\boldsymbol{\tau} + \boldsymbol{G}_{te}\boldsymbol{J}_{eb}\left(\boldsymbol{B}_b\boldsymbol{C}_b + \boldsymbol{B}_{bm}\boldsymbol{C}_m\right)\\ &\quad + \boldsymbol{G}_{te}\boldsymbol{J}_{em}\left(\boldsymbol{B}_{bm}^{\mathrm{T}}\boldsymbol{C}_b + \boldsymbol{B}_m\boldsymbol{C}_m\right) - \boldsymbol{G}_{te}\left(\dot{\boldsymbol{J}}_{eb}\boldsymbol{V}_0 + \dot{\boldsymbol{J}}_{em}\dot{\boldsymbol{q}}\right) - \boldsymbol{G}_t\boldsymbol{V}_t \times^* \boldsymbol{I}_t\boldsymbol{V}_t\\ &= -\boldsymbol{G}_{te}\boldsymbol{Ma}_e\boldsymbol{\tau} - \boldsymbol{G}_{te}\boldsymbol{b}_e - \boldsymbol{G}_t\boldsymbol{V}_t \times^* \boldsymbol{I}_t\boldsymbol{V}_t\\ &= \boldsymbol{Ma}_t\boldsymbol{\tau} + \boldsymbol{b}_t\end{aligned} \tag{35}$$

where $\boldsymbol{Ma}_t = -\boldsymbol{G}_{te}\boldsymbol{Ma}_e \in \mathbb{R}^{6\times N}$ is the dynamic manipulability matrix of the target. $\boldsymbol{b}_t = -\boldsymbol{G}_{te}\boldsymbol{b}_e - \boldsymbol{G}_t\boldsymbol{V}_t \times^* \boldsymbol{I}_t\boldsymbol{V}_t \in \mathbb{R}^6$ is the bias acceleration.

https://doi.org/10.1017/S0263574720000077 Published online by Cambridge University Press

Equation (35) can also be decomposed into angular and linear terms

$$\dot{\boldsymbol{V}}_t = \begin{bmatrix} \dot{\boldsymbol{\omega}}_t \\ \dot{\boldsymbol{v}}_t \end{bmatrix} = \begin{bmatrix} \boldsymbol{Ma}_t^{\omega} \\ \boldsymbol{Ma}_t^{\upsilon} \end{bmatrix} \boldsymbol{\tau} + \begin{bmatrix} \boldsymbol{b}_t^{\omega} \\ \boldsymbol{b}_t^{\upsilon} \end{bmatrix} \tag{36}$$

3.2. Dynamic manipulability measuring

3.2.1. Dynamic manipulability ellipsoid. The DME reflects the spatial distribution of dynamic manipulability. Taking $\boldsymbol{Ma}_t^{\omega}$ as the example, we can get the following expression from Eq. (36):

$$\boldsymbol{\tau} = \boldsymbol{Ma}_t^{\omega\,+}(\dot{\boldsymbol{\omega}}_t - \boldsymbol{b}_t^{\omega}) \tag{37}$$

where $+$ represents the pseudo-inverse. The joint torques are normalized as $\boldsymbol{\tau} = \boldsymbol{L}_{\tau}\hat{\boldsymbol{\tau}}$ using the weighting matrix $\boldsymbol{L}_{\tau} = \mathrm{diag}(|\tau_1|_{\max}, |\tau_2|_{\max}, \cdots, |\tau_N|_{\max})$, and Eq. (37) can be rewritten as

$$\hat{\boldsymbol{\tau}} = \boldsymbol{L}_{\tau}^{-1}\boldsymbol{Ma}_t^{\omega\,+}(\dot{\boldsymbol{\omega}}_t - \boldsymbol{b}_t^{\omega}) \tag{38}$$

If the normalized joint torques satisfy the unit sphere constraint $\|\hat{\boldsymbol{\tau}}\|_2 \le 1$, that is, $\hat{\boldsymbol{\tau}}^{\mathrm{T}}\hat{\boldsymbol{\tau}} \le 1$, the target's angular acceleration will satisfy the constraint

$$\begin{aligned} &(\dot{\boldsymbol{\omega}}_t - \boldsymbol{b}_t^{\omega})^{\mathrm{T}}(\boldsymbol{Ma}_t^{\omega\,+})^{\mathrm{T}}\boldsymbol{L}_{\tau}^{-2}\boldsymbol{Ma}_t^{\omega\,+}(\dot{\boldsymbol{\omega}}_t - \boldsymbol{b}_t^{\omega}) \le 1 \\ \text{or}\quad &(\dot{\boldsymbol{\omega}}_t - \boldsymbol{b}_t^{\omega})^{\mathrm{T}}(\boldsymbol{Ma}_t^{\omega}\boldsymbol{L}_{\tau}^{2}\boldsymbol{Ma}_t^{\omega\,\mathrm{T}})^{-1}(\dot{\boldsymbol{\omega}}_t - \boldsymbol{b}_t^{\omega}) \le 1 \end{aligned} \tag{39}$$

Eq. (39) expresses a 3-D ellipsoid constraint whose center is located in $\boldsymbol{b}_t^{\omega}$, which is called the target angular DME. The target linear DME and end-effector DME for the open-loop space robot can be defined in the similar way. The lengths of the three semi-axes of the ellipsoid are in proportion to the three singular values of $\boldsymbol{Ma}_t^{\omega}$, whose directions are the same with the corresponding eigenvectors. If the matrix has less than three nonzero singular values, the ellipsoid will become an ellipse in the plane or a pair of parallel lines.

The ellipsoidal volume (or the elliptical area) reflects the size of dynamic manipulability measure if the bias acceleration is omitted. However, the center of DME will deviate from the manipulation point due to the bias acceleration when the robotic system is moving, which makes the dynamic manipulability measure reduce in some directions while increase in opposite directions. Most seriously, the manipulation point can fall outside the ellipsoid and lose the ability to accelerate in most directions. The ellipsoidal volume (or elliptical area) cannot factually measure the dynamic manipulability under the circumstances.

3.2.2. Dynamic manipulability factor. The DMF considering the bias acceleration is proposed to compensate the defect of DME. $\boldsymbol{Ma}_t^{\omega}$ is still taken as the example, whose rank is r. Applying the singular value decomposition to it yields

$$\boldsymbol{Ma}_t^{\omega} = \begin{bmatrix} \boldsymbol{U}_1 & \boldsymbol{U}_2 \end{bmatrix} \begin{bmatrix} \boldsymbol{\Sigma} & \boldsymbol{0} \\ \boldsymbol{0} & \boldsymbol{0} \end{bmatrix} \begin{bmatrix} \boldsymbol{V}_1^{\mathrm{T}} \\ \boldsymbol{V}_2^{\mathrm{T}} \end{bmatrix} \tag{40}$$

where $\boldsymbol{U}_1 \in \mathbb{R}^{3\times r}$, $\boldsymbol{U}_2 \in \mathbb{R}^{3\times(3-r)}$, $\boldsymbol{V}_1 \in \mathbb{R}^{N\times r}$, $\boldsymbol{V}_2 \in \mathbb{R}^{N\times(N-r)}$. $\boldsymbol{\Sigma} = \mathrm{diag}(\sigma_1, \sigma_2, \cdots, \sigma_r) \in \mathbb{R}^{r\times r}$ is the diagonal matrix consisting of all nonzero singular values of $\boldsymbol{Co}_{bm}^{\omega}$. The target angular DMF without offset is defined as

$$v_t^{\omega} = \sigma_1(\boldsymbol{Ma}_t^{\omega})\sigma_2(\boldsymbol{Ma}_t^{\omega})\cdots\sigma_r(\boldsymbol{Ma}_t^{\omega}) = \det(\Sigma(\boldsymbol{Ma}_t^{\omega})) \tag{41}$$

When the robotic system is in a static state, the DMF is the product of the three (or less) singular values of the dynamic manipulability matrix, therefore proportional to the corresponding ellipsoidal volume (or the elliptic area). As mentioned earlier, it cannot factually reflect the dynamic manipulability when the bias acceleration exists. So the bias factor is defined

$$\eta = \sqrt{\left(\frac{(\boldsymbol{p}_t^{\omega})_x}{\sigma_1}\right)^2 + \left(\frac{(\boldsymbol{p}_t^{\omega})_y}{\sigma_2}\right)^2 + \left(\frac{(\boldsymbol{p}_t^{\omega})_z}{\sigma_3}\right)^2} \tag{42}$$

https://doi.org/10.1017/S0263574720000077 Published online by Cambridge University Press

Table II. Kinematic and dynamic parameters of the dual-arm space robot.

Number	**0**	**1**	**2**	**3**	**4**	**5**	**6**	$e(1)$	$e(2)$
$\lambda(i)$	–	0	1	2	0	4	5	–	–
The end	No	No	No	Yes	No	No	Yes	–	–
Joint type	–	R	R	R	R	R	R	–	–
m_i, kg	100	10	10	10	10	10	10	–	–
$\bar{I}_{xx}$, $kg \cdot m^2$	10	1	1	1	1	1	1	–	–
$\bar{I}_{yy}$, $kg \cdot m^2$	10	1	0.1	0.1	1	0.1	0.1	–	–
$\bar{I}_{zz}$, $kg \cdot m^2$	10	0.1	1	1	0.1	1	1	–	–
α_i, rad	–	0	0	0	0	0	0	0	0
β_i, rad	–	0	0	0	0	0	0	0	0
γ_i, rad	–	0	0	0	0	0	0	0	0
r_x, m	–	0	0	0	0	0	0	0	0
r_y, m	–	−1	−1	−1	1	1	1	−1	1
r_z, m	–	0	0	0	0	0	0	0	0
c_x, m	0	0	0	0	0	0	0	–	–
c_y, m	0	−0.5	−0.5	−0.5	0.5	0.5	0.5	–	–
c_z, m	0	0	0	0	0	0	0	–	–

where $\boldsymbol{p}_t^{\omega} = \boldsymbol{U}^{-1}\boldsymbol{b}_t^{\omega}$ is the bias acceleration in the ellipsoidal frame. If $\boldsymbol{M}\boldsymbol{a}_t^{\omega}$ is rank deficit, we can only take the first two or one terms. η measures the offset between the ellipsoidal origin and the manipulation point. The relationship between η and the position of the manipulation point is

$$\eta \begin{cases} < 1, & \text{the manipulation point is inside the ellipsoid} \\ = 1, & \text{the manipulation point is on the edge} \\ > 1, & \text{the manipulation point is outside the ellipsoid} \end{cases} \tag{43}$$

when $\eta \geq 1$, the manipulation point is not inside the ellipsoid and the dynamic manipulability is lost. The new DMF considering the offset is defined as

$$v_t^{\omega} = \begin{cases} (1-\eta)\det(\Sigma(\boldsymbol{M}\boldsymbol{a}_t^{\omega})), & \eta < 1 \\ 0, & \eta \geq 1 \end{cases} \tag{44}$$

The DMF for other cases can be defined similarly.

4. Dynamic Manipulability Simulation and Analysis

In this section, the rigid bodies of robotic system are assumed to be resting firstly, that is, the bias acceleration is ignored, where the effects of dynamic parameters, link lengths, and joint configurations are considered. Then the effects of joint velocities on the dynamic manipulability measure are explored.

4.1. Dynamic manipulability without bias acceleration

4.1.1. Effects of mass. The dynamic manipulability of the open-loop space robot is considered first. Table II presents the initial kinematic and dynamic parameters of a dual-arm space robot, where 0 is the base and $e(1)$ and $e(2)$ represent the two end-effectors. All vectors and matrices are expressed in their fixed body frame, noticing that the Euler angles and $\boldsymbol{r}_i$ are fixed with body $\lambda(i)$ rather than body i. The schematic of the robotic system is shown in Fig. 3.

To analyze the effects of each body's mass on the dynamic manipulability, we view them as independent variables and let them increase from 1 to 100 kg, respectively (the rotational inertia increases in the same proportion), while the mass of other bodies stays the same. The DMFs are used as dependent variables. Two joint configurations (1) Case 1: $\boldsymbol{q} = [-\pi/6, -\pi/3, -\pi/3, \pi/6, \pi/3, \pi/3]^{\mathrm{T}}$ and (2) Case 2: $\boldsymbol{q} = [\pi/6, -2\pi/3, -\pi/3, -\pi/6, 2\pi/3, \pi/3]^{\mathrm{T}}$ are set here. The space robot is moving in the plane, and the base has an angular and two linear degrees of freedom. Since the joint configuration is symmetrical, we just investigate the left arm's dynamic manipulability. The simulation

https://doi.org/10.1017/S0263574720000077 Published online by Cambridge University Press

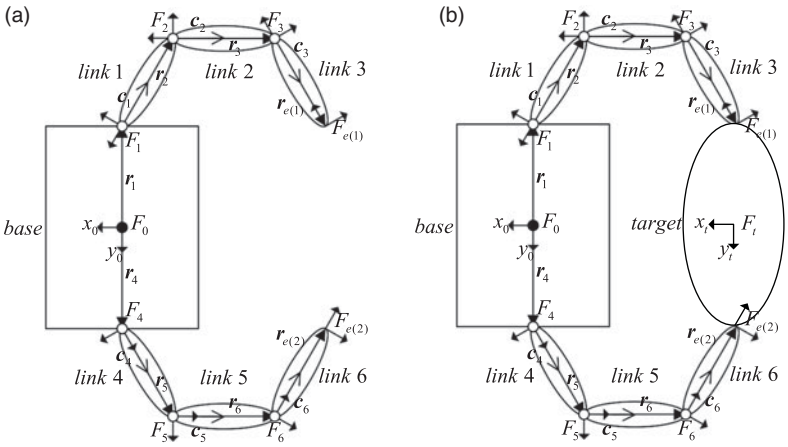

The open-loop space robot before capture The closed-loop system after capture

Fig. 3. Schematic of a free-floating dual-arm space robotic system.

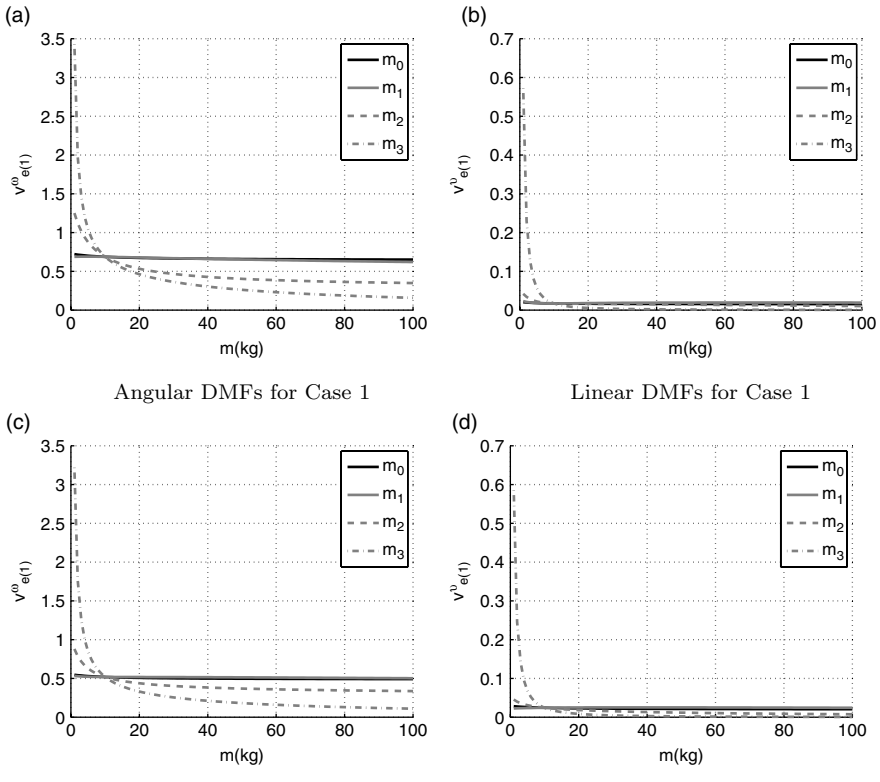

Angular DMFs for Case 1 Linear DMFs for Case 1

Angular DMFs for Case 2 Linear DMFs for Case 2

Fig. 4. Left-end DMFs for the open-loop space robot with respect to mass.

results are shown in Fig. 4. The increase of the mass of rigid bodies reduces the end-effector dynamic manipulability to varying degrees, while the DMFs are most sensitive to the mass change of link 3.

Above methods are promoted to the closed-loop system. The model is composed of the dual-arm space robot and a captured target whose mass m_t and rotational inertia $\bar{\boldsymbol{I}}_t$ change in the same way. As shown in Fig. 3, the target frame is in the same direction as the space robot base frame, and the distances from the two capture points are 1 m. Figure 5 shows the simulation results for two joint configuration cases. The target DMFs are negatively correlated with the mass of all rigid bodies besides link 1. The target angular DMF increases with the increase of m_1 at first, and the tendency to decrease appears when $m_1 \geq 40$ kg.

https://doi.org/10.1017/S0263574720000077 Published online by Cambridge University Press

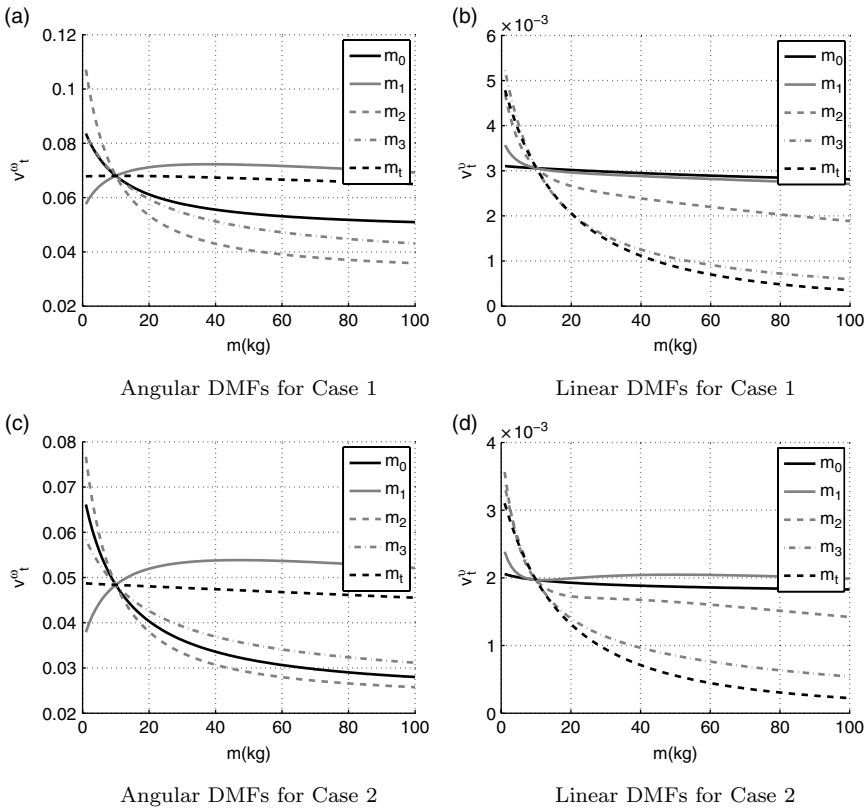

Angular DMFs for Case 1 | Linear DMFs for Case 1

Angular DMFs for Case 2 | Linear DMFs for Case 2

Fig. 5. Target DMFs for the closed-loop system with respect to mass.

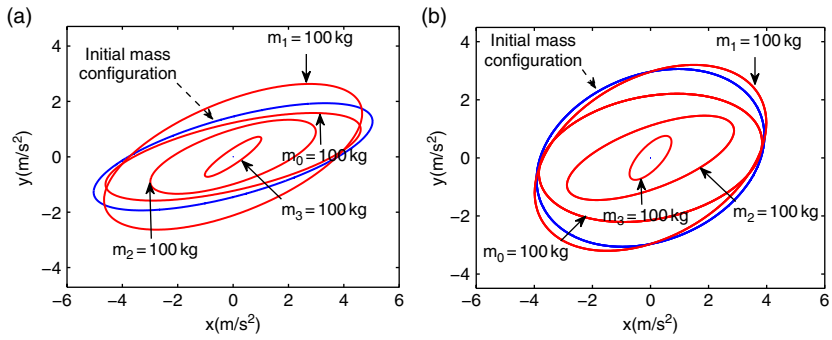

Linear DMEs for Case 1 | Linear DMEs for Case 2

Fig. 6. Left-end DMEs for the open-loop space robot with respect to mass.

The spatial distribution of dynamic manipulability can be further illustrated by DMEs. Since the base moves in the plane, we only consider the linear DMEs here. The weighting matrix is $\boldsymbol{L}_\tau = \text{diag}(50, 25, 10, 50, 25, 10)$. The simulation results for the open-loop space robot is shown in Fig. 6, which are expressed in the base coordinate frame. The mass of the base and each link of the left arm increases to 100 kg successively and is compared with the initial mass configuration where the mass of each body is 10 kg. The increase of mass for all rigid bodies makes the elliptical directions biased toward corresponding bodies. When the mass of link 1 increases to 100 kg, the corresponding linear DMEs are not much changed from the initial mass configuration in area. The DMEs corresponding to other conditions are smaller than the initial condition, where the DMEs for $m_3 = 100$ kg are smallest, which are consistent with preceding DMF analysis. The dynamic manipulability along the tangential direction is much larger than that along the normal direction in all conditions.

As for the closed-loop system under the same joint configurations, the mass of the base, each link of the left arm, and target is increased to 100 kg in order, the corresponding DMEs are compared with

https://doi.org/10.1017/S0263574720000077 Published online by Cambridge University Press

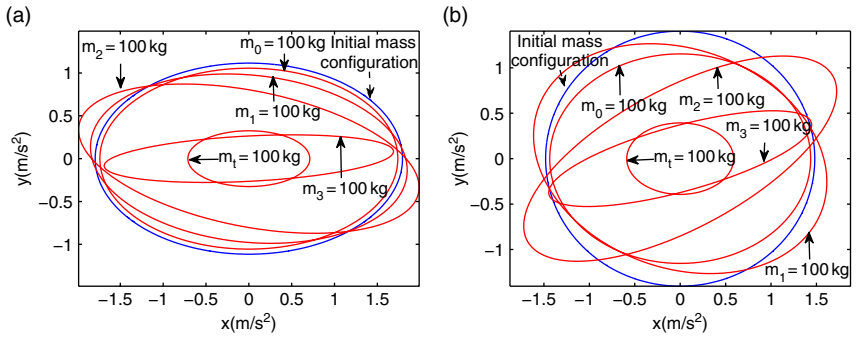

Linear DMEs for Case 1 Linear DMEs for Case 2

Fig. 7. Target DMEs for the closed-loop system with respect to mass.

the initial mass configuration. The simulation results are shown in Fig. 7, which are also expressed in the base coordinate frame. The mass changes of the base and target have no effect on the elliptical directions, while those of the left arm bodies make the elliptical directions biased. The elliptical areas reduce when the mass of all bodies increases, and the closer the body to the target, the smaller the DME is.

Overall, above simulations for the open-loop and closed-loop systems show that the dynamic manipulability is negatively correlated with the mass of rigid bodies in most cases. From this point of view, the weight of links close to the end should be lighten to increase its dynamic manipulability when designing dynamics parameters. However, the end links ought to have a certain weight to avoid damage during tasks. Both sides should be considered in practice.

4.1.2. Effects of link lengths. The dynamic manipulability is also affected by kinematic parameters like the lengths of links. In the previous study, the link lengths are unified as 1 m, and we will investigate the effects of link lengths in this subsection. The simulation methods of the open-loop space robot are similar to those for the open-loop space robot in the last subsection, where the variation tendency of DMFs with the change of link lengths will be viewed. The mass and inertia of all bodies remain unchanged as Table II, and the length of each link increases from 0.1 to 10 m, while its CoM is always located in the midpoint of the link. Two joint configurations (1) Case 1: $\boldsymbol{q} = [-\pi/6, -\pi/3, -\pi/3, \pi/6, \pi/3, \pi/3]^{\mathrm{T}}$ and (2) Case 2: $\boldsymbol{q} = [\pi/6, -2\pi/3, -\pi/3, -\pi/6, 2\pi/3, \pi/3]^{\mathrm{T}}$ are considered here. The simulation results are shown in Fig. 8. It can be seen that the DMFs decrease as the links lengthen on the whole, while it may slightly increase when the links are very short.

Based on the above performance, the dynamic manipulability degrees decline rapidly with respect to the length of links. It is unfavorable to be too long when designing kinematic parameters. However, the links also should not be too short to ensure adequate workspace.

4.1.3. Effects of joint variables. In this subsection, the joint variables are viewed as independent variable to study their effects on the dynamic manipulability. The dynamic manipulability characteristic can behave specially when the system is near a singular configuration, for example, the manipulators are outstretched or contracted. They are difficult to move in some directions under these circumstances. To view the performance of dynamic manipulability near the singular configuration, we use the open-loop space robot in Table II and observe the DMFs with respect to the change of q_2 and q_3, respectively, while other joint variables remain zero. The results are shown in Fig. 9. The angular DMFs rise rapidly to its maximum values when q_2 or q_3 is near 0° or 180° (the manipulator is outstretched or contracted), while drops rapidly to the minimum values when q_2 or q_3 is near 90° or 270°. The variation tendency of the linear DMFs is completely opposite, which drop very fast to zero when the robotic system is very close to the singular configuration.

According to the definition of the correlation matrices, let each joint variable changes from 0° to 360° successively, and the DMFs under all joint variable combinations are obtained. On this basis, we can draw DMF maps which can visually reflect the dynamic manipulability under different joint variables. Since the number of joint variables combinations is too large for a high-degree system

https://doi.org/10.1017/S0263574720000077 Published online by Cambridge University Press

Table III. Kinematic and dynamic parameters of the single-arm space robot.

Number	**0**	**1**	**2**	***e***
$\lambda(i)$	–	0	1	–
The end	No	No	Yes	–
Joint type	–	R	R	–
m_i, kg	10	10	10	–
$\bar{\boldsymbol{I}}_i$, $kg \cdot m^2$	diag(1,1,1)	diag(1,1,0.1)	diag(1,0.1,1)	–
α_i, β_i, γ_i, rad	–	$[0\ 0\ 0]^{\mathrm{T}}$	$[0\ 0\ 0]^{\mathrm{T}}$	$[0\ 0\ 0]^{\mathrm{T}}$
$\boldsymbol{r}_i$, m	–	$[0\ 1\ 0]^{\mathrm{T}}$	$[0\ 1\ 0]^{\mathrm{T}}$	$[0\ 1\ 0]^{\mathrm{T}}$
$\boldsymbol{c}_i$, m	–	$[0\ 0.5\ 0]^{\mathrm{T}}$	$[0\ 0.5\ 0]^{\mathrm{T}}$	$[0\ 0.5\ 0]^{\mathrm{T}}$

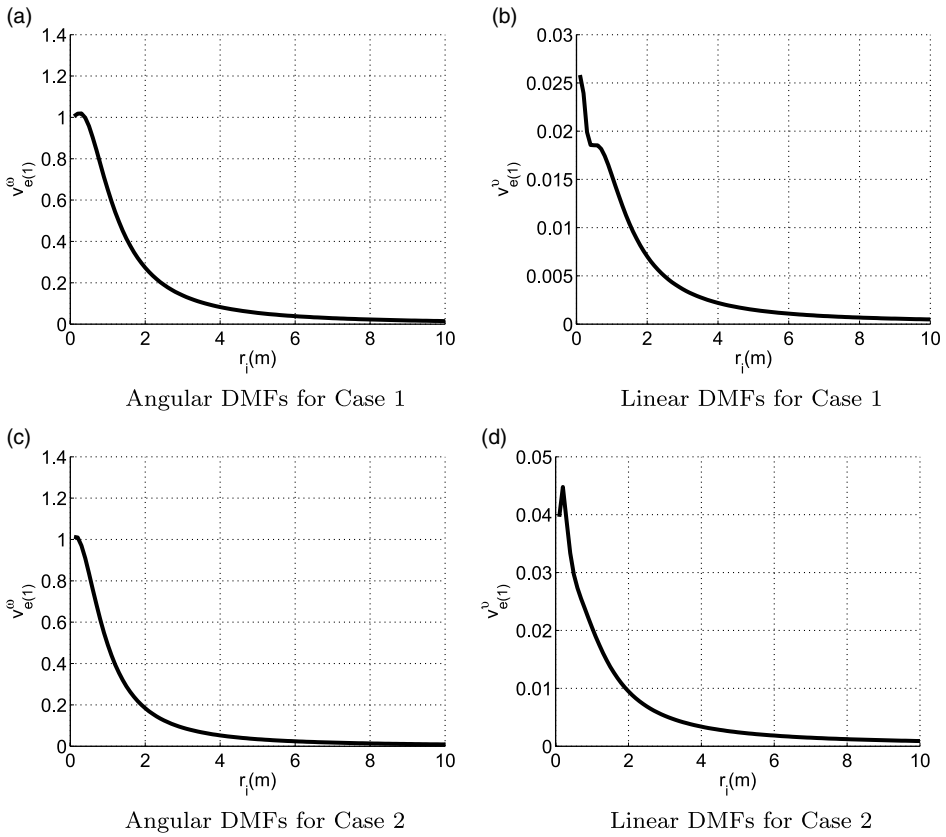

Fig. 8. Left end DMFs for the open-loop space robot with respect to link lengths.

(link number is three or more), here we use a two-link single-arm space robot as the research model for simplicity, whose parameters are shown in Table III.

The DMF maps are shown in Figs. 10 and 11, where the mass of each body increases to 100 kg, and maps under different mass configurations are compared. It is shown that the increase in mass makes DMFs reduce in varying degrees, where DMFs for the condition of $m_2 = 100$ kg are much lower than the original state, which is consistent with foregoing research. Noticing that when q_2 is around 0° or 360°, that is, the manipulator is outstretched, the end-effector's angular DMFs are much larger, while its linear DMFs are much smaller than other regions. For the area where q_2 is around 180°, that is, the manipulator is constrictive, both the angular and linear DMFs are lower.

The DMF maps under all joint variables have great significance for the trajectory planning of free-floating space robots. From which we can visually see the joint variable area of large or small DMFs, and let the manipulator move along the paths with larger DMF. As for systems with high degrees of freedom, the DMF maps associated with joint variables are difficult to get, while the DMF can still be

https://doi.org/10.1017/S0263574720000077 Published online by Cambridge University Press

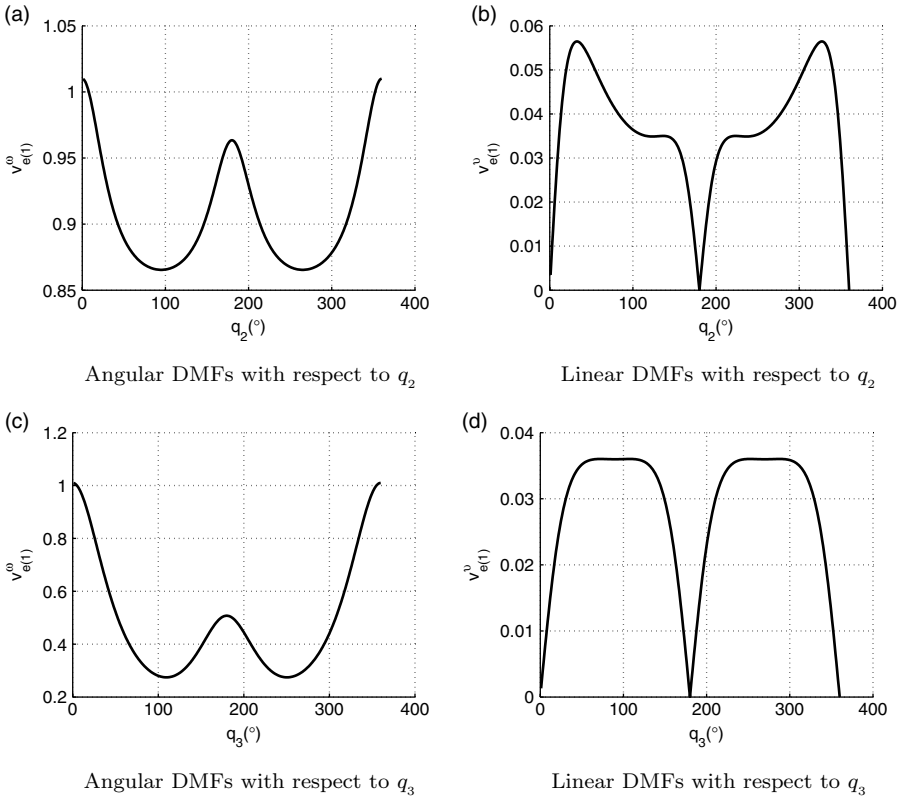

Angular DMFs with respect to q_2 Linear DMFs with respect to q_2

Angular DMFs with respect to q_3 Linear DMFs with respect to q_3

Fig. 9. Left-end DMFs for the open-loop space robot with respect to joint variables.

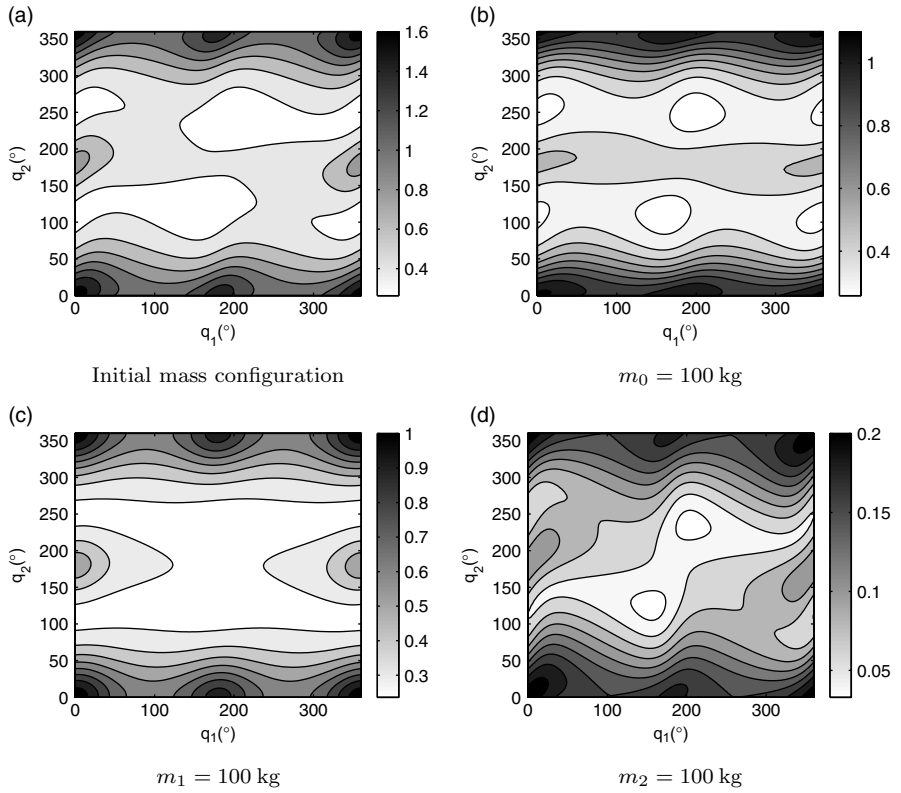

Initial mass configuration $m_0 = 100$ kg

$m_1 = 100$ kg $m_2 = 100$ kg

Fig. 10. End angular DMF maps under different mass configurations.

https://doi.org/10.1017/S0263574720000077 Published online by Cambridge University Press

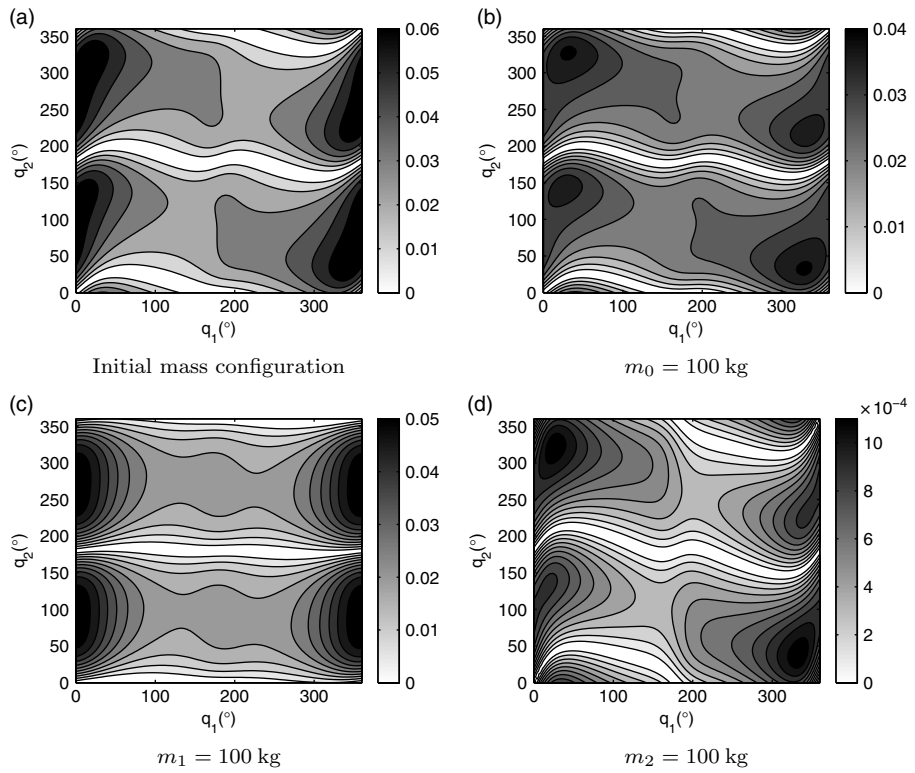

Fig. 11. End linear DMF maps under different mass configurations.

used as an optimization index to maximize the manipulator's performance. The trajectory planning problem can be stated as the following optimization problem under a list of inequality constraints $g_i(\boldsymbol{q})$ and equality constraints $h_i(\boldsymbol{q})$:

$$\begin{aligned} &\text{maximize}: v_e(\boldsymbol{q}) \quad \text{or} \quad v_t(\boldsymbol{q}) \\ &\text{subject to}: g_i(\boldsymbol{q}) < 0,\ i = 1, 2, \cdots, n_{ieq} \\ &\qquad\qquad h_i(\boldsymbol{q}) = 0,\ i = 1, 2, \cdots, n_{eq} \end{aligned} \tag{45}$$

4.2. Dynamic manipulability with bias acceleration

When the manipulators move, the manipulation point will obtain different dynamic manipulability in opposite directions due to the bias acceleration, which depends on joint velocities. According to the definition of bias acceleration, it has a quadratic relationship with joint velocities. Firstly, the effects of joint velocities on DMFs are investigated. For the dual-arm space robot in Table II, the simulation results for the changes of left-end DMFs with joint velocities under different mass configurations are shown in Fig. 12. It can be seen that the DMFs decline quadratically with joint velocities. Noticing that the stationary DMFs on the conditions of $m_0 = 100$ kg and $m_1 = 100$ kg are larger, but fall faster with the increase of joint velocities. On the contrary, the DMFs for $m_2 = 100$ kg and $m_3 = 100$ kg are lower in a static state but decline slower with joint velocities.

The effects of bias accelerations can be further illustrated by DMEs. The simulation results for the left-end DMEs under different mass configurations are shown in Fig. 13, where all joint velocities q_i, $i = 1, \cdots, N$ are 1 rad/s. The arrows represent the bias acceleration vectors from the manipulation point to ellipsoidal centers, which are also expressed in the base frame. Compare it to Fig. 6, almost all DMEs are completely deviated from the manipulation point, meaning that it cannot be accelerated in most directions. The DMEs for $m_0 = 100$ kg and $m_1 = 100$ kg are larger but have farther deviation distance. Meanwhile, those for $m_2 = 100$ kg and $m_3 = 100$ kg are smaller but closer to the manipulation point, which confirms the previous results.

https://doi.org/10.1017/S0263574720000077 Published online by Cambridge University Press

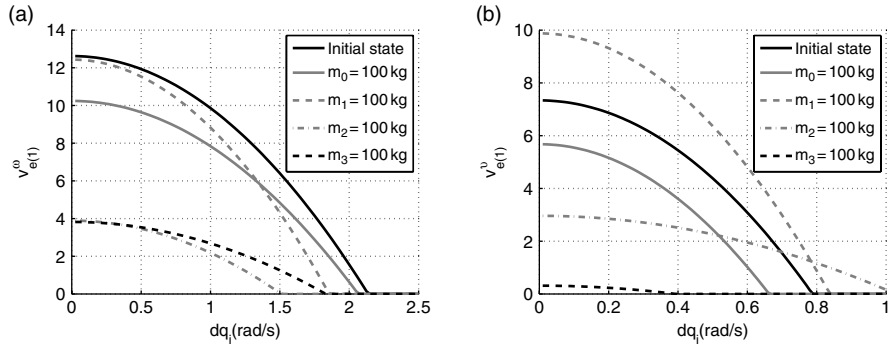

Angular DMFs for Case 1 Linear DMFs for Case 1

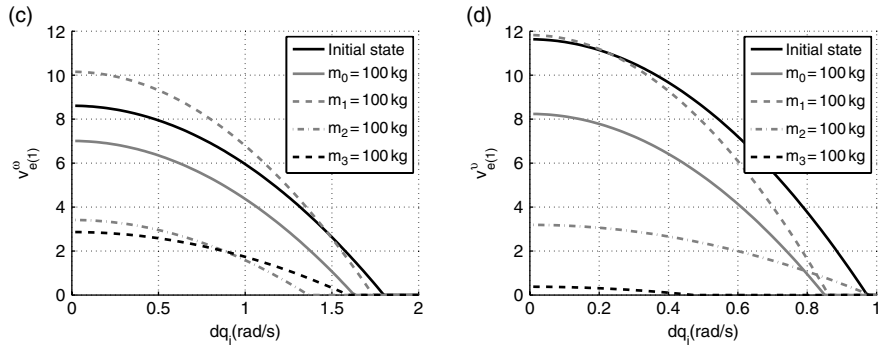

Angular DMFs for Case 2 Linear DMFs for Case 2

Fig. 12. Left-end DMFs for the open-loop space robot with joint velocities.

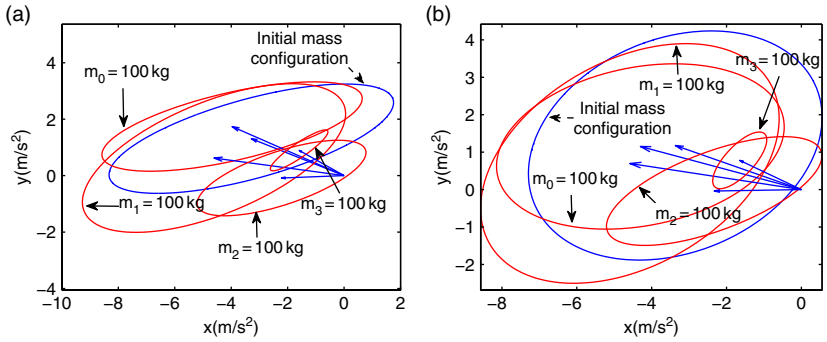

Linear DMEs for Case 1 Linear DMEs for Case 2

Fig. 13. Left-end DMEs for the open-loop space robot when joint velocities are 1 rad/s.

5. Conclusions

The dynamic manipulability is one of the most important indicators for the manipulator. Previous studies have mainly focused on the ground fixed-base manipulator, while that for the space robot has not been investigated. The main features of this paper can be listed as follows:

1. The dynamic manipulability of the open-loop multi-arm space robot is studied and further expanded to its combined closed-loop system with the captured target.
2. The spatial vector theory and the graph theory are used to model general space robots, which are appropriate for a serial space robot with arbitrary configuration. On the basis of dynamic manipulability modeling, the DME and DMF considering bias accelerations are proposed as two indicators for dynamic manipulability measure.

https://doi.org/10.1017/S0263574720000077 Published online by Cambridge University Press

3. For the open-loop space robot and the closed-loop system under static state, the effects of dynamic parameters, link lengths, and joint variables are mainly studied using above indicators. Then, the effects of joint velocities are explored taking the bias acceleration into account.

The results can be used as an important reference for the dynamics parameters design and trajectory planning. Joint trajectories with higher dynamic manipulability can be chosen for a single manipulator through the DMF maps. As for high-degree systems, the proposed dynamic manipulability measure can be used as an optimization index, which will be one of our future work.

Acknowledgments

This research was supported by "The National Natural Science Foundation of China (Grant Nos. 61603304, 61690210 and 61690211)" and "Qingdao Innovation Programme (Grant No. 18-2-2-14-jch)."

References

1. K. Doetsch, "Canada's role on space station," *Acta Astronaut.* **57**(2), 661–675 (2005).
2. G. Hirzinger, K. L. Landzettel and J. Heindl, "ROTEX: Space telerobotic flight experiment," *Telemanipulator Technol. Space Telerobot.* **2057**, 51–72 (1993).
3. M. Oda, "Ground-space bilateral teleoperation of ETS-VII robot arm by direct coupling under 7-s time delay condition," *IEEE Trans. Robot. Autom.* **20**(3), 499–511 (2004).
4. R. O. Ambrose, H. Aldridge, R. S. Askew, R. R. Burridge, W. Bluethmann, M. Diftler, C. Lovchik, D. Magruder and F. Rehnmark, "Robonaut: NASA's space humanoid," *IEEE Intell. Syst. Appl.* **15**(4), 57–63 (2000).
5. G. V. Tzvetkova, "Robonaut 2: Mission, technologies, perspectives," *J. Theor. Appl. Mech.* **44**(1), 97–102 (2014).
6. G. Rouleau, I. Rekleitis, R. L'Archeveque, E. Martin, K. Parsa and E. Dupuis, "Autonomous capture of a tumbling satellite," *J. Field Robot.* **24**(4), 275–296 (2007).
7. A. F. Abad, Z. Wei, O. Ma and K. Pham, "Optimal control of space robots for capturing a tumbling object with uncertainties," *J. Guidance Cont. Dyn.* **37**(6), 2014–2017 (2014).
8. T. Yoshikawa, "Manipulability of robotic mechanisms," *Int. J. Robot. Res.* **4**(2), 3–9 (1985).
9. N. Vahrenkamp, T. Asfour, G. Metta, G. Sandini and R. Dillmann, "Manipulability analysis," *IEEE-RAS International Conference on Humanoid Robots* (2012) pp. 568–573.
10. N. Vahrenkamp and T. Asfour, "Representing the robot's workspace through constrained manipulability analysis," *Auton. Robots* 38 (1), 17–30 (2015).
11. T. Okada and K. Tahara, "Development of a two-link planar manipulator with continuously variable transmission mechanism," *IEEE/ASME International Conference on Advanced Intelligent Mechatronics* (2014) pp. 617–622.
12. Y. Tanaka, K. Nishikawa, N. Yamada and T. Tsuji, "Analysis of operational comfort in manual tasks using human force manipulability measure," *IEEE Trans. Haptics* **8**(1), 8–19 (2015).
13. M. Wang, J. Luo and U. Walter, "Trajectory planning of free-floating space robot using Particle Swarm Optimization (PSO)," *Acta Astronaut.* **112**, 77–88 (2015).
14. M. Wang, J. Luo, J. Fang and J. Yuan, "Optimal trajectory planning of free-floating space manipulator using differential evolution algorithm," *Adv. Space Res.* 61, 1525–1536 (2018).
15. M. Wang, J. Luo, J. Yuan and U. Walter, "Coordinated trajectory planning of dual-arm space robot using constrained particle swarm optimization," *Acta Astronaut.* **146**, 259–272 (2018).
16. X. Chen and S. Qin, "Motion planning for dual-arm space robot towards capturing target satellite and keeping the base inertially fixed," *IEEE Access* **6**, 26292–26306 (2018).
17. L. Yan, W. Xu, Z. Hu and B. Liang, "Virtual-base modeling and coordinated control of a dual-arm space robot for target capturing and manipulation," *Multibody Syst. Dyn.* **45**(4), 431–455 (2019).
18. L. Yan, H. Yuan, W. Xu, Z. Hu and B. Liang, "Generalized relative jacobian matrix of space robot for dual-arm coordinated capture," *J. Guidance Cont. Dyn.* **41**(5), 1202–1208 (2018).
19. B. Zhang, B. Liang and X. Wang, "Target Manipulation Ability of Space Robot in Post-capture Phase," *27th Chinese Control and Decision Conference (CCDC)* (2015) pp. 2596–2601.
20. B. Zhang, B. Liang, X. Wang, G. Li, Z. Chen and X. Zhu, "Manipulability measure of dual-arm space robot and its application to design an optimal configuration," *Acta Astronaut.* **128**, 322–329 (2016).
21. T. Yoshikawa, "Dynamic manipulability of robot manipulators," *J. Robot. Syst.* **2**(1), 113–124 (1985).
22. P. Chiacchio, "A new dynamic manipulability ellipsoid for redundant manipulators," *Robotica* **18**(7), 381–387 (2000).
23. M. T. Rosenstein and R. A. Grupen, "Velocity-Dependent Dynamic Manipulability," *IEEE International Conference on Robotics & Automation*, (2002) pp. 2424–2429.
24. P. Chiacchio, S. Chiaverini, L. Sciavicco and B. Siciliano, "Global task space manipulability ellipsoids for multiple-arm systems," *IEEE Trans. Robot. Autom.* **7**(5), 678–685 (1991).
25. J. Lee and H. Shim, "On the Dynamic Manipulability of Cooperating Multiple Arm Robot Systems," *IEEE/RSJ International Conference on Intelligent Robots & Systems* (2004) pp. 2087–2092.

26. Y. Yokokohji, J. S. Martin and M. Fujiwara, "Dynamic manipulability of multifingered grasping," *IEEE Trans. Robot.* **25**(4), 947–954 (2009).
27. S. Cotton, P. Fraisse and A. Murray, "On the Manipulability of the Center of Mass of Humanoid Robots: Application to Design," *ASME International Design Engineering Technical Conferences & Computers & Information in Engineering Conference* (2010) pp. 1259–1267.
28. Y. Gu, C. Lee and B. Yao, "Feasible Center of Mass Dynamic Manipulability of Humanoid Robots," *IEEE International Conference on Robotics and Automation* (2015) pp. 5082–5087.
29. M. Azad, J. Babic and M. Mistry, "Dynamic Manipulability of the Center of Mass: A Tool to Study, Analyse and Measure Physical Ability of Robots," *IEEE International Conference on Robotics and Automation (ICRA)* (2017) pp. 3484–3490.
30. M. Minami, X. Li, T. Matsuno and A. Yanou, "Dynamic reconfiguration manipulability for redundant manipulators," *J. Robot. Soc. Japan* **34**(4), 272–279 (2016).
31. K. Shen, X. Li, H. Tian, D. Izawa, M. Minami and T. Matsuno, "Application and Analyses of Dynamic Reconfiguration Manipulability Shape Index into Humanoid Biped Walking," *IEEE International Conference on Robotics and Biomimetics* (2016) pp. 1436–1441.
32. M. Azad, J. Babič and M. Mistry, "Effects of the weighting matrix on dynamic manipulability of robots," *Auton. Robots* **43**(7), 1867–1879 (2019).
33. R. Featherstone, "A beginner's guide to 6-D vectors (Part 1)," *Robot. Autom. Mag.* IEEE **17**(3), 83–94 (2010).
34. R. Featherstone, "A beginner's guide to 6-D vectors (part 2)," *IEEE Robot. & Autom. Mag.* **17**(4), 88–99 (2010).

https://doi.org/10.1017/S0263574720000077 Published online by Cambridge University Press